Int. J. Therm. Sci. (2001) 40, 550–563

S1290-0729(01)01243-1/FLA

Heat transfer processes during an unfixed solid phase change material melting outside a horizontal tube

Yingxin Zhu, Yinping Zhang, Gang Li, Fengjun Yang

Department of Building Science and Technology, School of Architecture, Tsinghua University, Beijing 100084, PR China

(Received 7 June 2000, accepted 23 August 2000)

Abstract — The melting of an unrestrained phase change material (PCM) around a horizontal tube arises in many applications such as ice storage for HVAC (Heating, Ventilating and Air Conditioning) systems. The instantaneous heat transfer rate during the melting process must be known for optimal system design and operation of the application. A theoretical model was developed to analyze the heat transfer during the melting process. A series of experiments on internal melting of unrestrained ice around a fixed horizontal tube were reported. The temporal geometric shape, melting rates under various experimental conditions were determined using a photograph technique. The experimental results were used to validate the theoretical model. The validation results show that the model accurately predicts the solid PCM melting rate. © 2001 Éditions scientifiques et médicales Elsevier SAS

phase change material / thermal storage / melting / heat transfer / modeling

Nomenclature

a	liquid phase thermal diffusivity	$m^2 \cdot s^{-1}$
c_p	liquid phase specific heat	$kJ \cdot kg^{-1} \cdot K^{-1}$
d	diameter	m
g	gravitational acceleration	$m \cdot s^{-2}$
h	convective heat transfer coefficient	$W \cdot m^{-2} \cdot K^{-1}$
h_{fus}	latent heat of fusion	$J \cdot kg^{-1}$
k	thermal conductivity	$W \cdot m^{-1} \cdot K^{-1}$
L	length of the solid phase cylinder	m
l	thickness of the solid PCM cylinder	m
p	liquid pressure difference between the melted layer and outside of the solid at the same height	Pa
Pr	Prandtl number	
Pe	Peclet number	
q''	heat flux	$W \cdot m^{-2}$
q	total heat transfer or melting rate	W
Re	Reynolds number	
R	tube outer radius	m
R_i	tube inner radius	m
R_s	solidified PCM cylinder outside radius	m
Ste	Stephan number $= c_p(T_w - T_m)/h_{fus}$	
S	shift of the solid PCM shell	m
T	temperature	°C
u	tangential velocity	$m \cdot s^{-1}$
$\overline{u}$	average tangential velocity in the melted film in contact region	$m \cdot s^{-1}$
v	normal velocity	$m \cdot s^{-1}$
x	coordinate tangential to the tube	m
y	coordinate normal to the tube	m
U^n	vertical solid velocity at instant τ^n	$m \cdot s^{-1}$
U^{n*}	dimensionless vertical solid velocity at instant τ^n, $= U^n \rho^* R/a$	

Greek symbols

μ	liquid phase dynamic viscosity	$kg \cdot m^{-1} \cdot s^{-1}$
ν	liquid phase kinematic viscosity	$m^2 \cdot s^{-1}$
τ	time	s
τ_{yx}	melted layer shear stress	$N \cdot m^{-2}$
δ	melted layer thickness	m
δ_w	tube wall thickness $= R - R_t$	m
Δ^*	dimensionless melted layer thickness	
ρ	density	$kg \cdot m^{-3}$
ρ^*	solid–liquid density ratio $= \rho_s/\rho_l$	
$\Delta\rho$	solid–liquid density difference $= \lvert\rho_l - \rho_s\rvert$	$kg \cdot m^{-3}$
ξ	correction factor for dimensionless vertical solid velocity after the solid is penetrated	
ϕ	angle of perimeter of contact region	
ϕ_{cri}	critical angle for the extent to which $\Delta^* \ll 1$	

E-mail address: Zhuyx@mail.tsinghua.edu.cn (Y. Zhu).

θ angle of perimeter for remote region zone A
Θ angular extent of remote region zone B

Superscripts

n order of instant $\tau = \tau^n$
$*$ dimensionless quantity

Subscripts

f heating fluid
i inside of the tube or cylinder
o outside of the tube or cylinder
contact contact region
l liquid phase
m melting point
s solid phase
w tube wall

1. INTRODUCTION

Melting phenomena are frequently encountered in processes such as casting of metals, freeze-drying of foodstuffs, growth of pure crystals from melts and solutions, freezing and thawing of moist soil, and latent heat thermal energy storage. In recent years, the use of ice storage systems for HVAC (Heating, Ventilation and Air Conditioning) applications has attracted increasing attention due to the desire to shift peak electrical loads. For such systems, the characteristics of the charging or discharging processes must be thoroughly understood for optimal design and operation of the system. Therefore, the study of the heat transfer characteristics of latent heat storage units with various configurations and operation conditions is of growing interests.

Heat transfer phenomena accompanying the phase change process above and below a heated horizontal flat plate and along a vertical surface were studied by Hale and Viskanta [1, 2]. The phase change process around a single cylinder or an array of horizontal cylinders (finned or unfinned) was the subject of several experimental investigations [3–6]. Rieger et al. [7] successfully solved this problem numerically. The melting process inside cylindrical enclosures has been studied extensively as well. The vertical arrangement was investigated experimentally by Bareiss and Beer [8] and the horizontal configuration has been the subject of numerical [9], experimental [10] and combined [11] studies. The common feature of these investigations with regard to the melting process inside a horizontal heated tube is that the location of the solid phase change material (PCM) was fixed during melting. If the solid PCM is free to move it will sink to the bottom (if inside a tube) or sink so that it is always resting on the tube if the PCM is around the tube due to the gravitational force or buoyancy resulting from the difference between the solid and liquid densities. This movement will have a significant impact on the melting process. Bahrami et al., Shi et al., and Moalemi et al. studied the contact melting problems [12–21]. Nicholas et al. [18] numerically analyzed the melting of unfixed solid PCM in a horizontal tube by solving the governing equations with a finite-difference method. However, their experimental results were only used for qualitative comparisons. Bareiss and Beer [19] studied a similar problem theoretically and experimentally. Their analytical results are in good agreement with the experimental results. It should be point out that the lubrication theory approximation was applied the first time by Bareiss et al. [19] and since then the approximation is the basis of all direct-contact melting considerations. Cheng et al. [20, 21] analyzed the melting of unfixed PCM in a tube with an oval cross section and in a tube with a rectangular cross section. However, as far as we know, melting of unfixed solid PCM around a horizontal tube has not been thoroughly studied in spite of a series of experimental studies about this process have been reported by Webb [17] and Yang [22]. This present paper presents a new model for analyzing the melting of an unfixed solid PCM around a horizontal tube.

2. ANALYSIS

The physical model considers a horizontal tube with a given length embedded in the solidified PCM cylinder (*figure 1(a)*). A heating fluid flows in the tube. The tube is fixed and the PCM cylinder can move up or down during melting due to the solid–liquid density difference. The solid temperature is at its melting temperature and the thermal resistance of the tube wall is negligible.

The properties of ice and water are used for the PCM in the analysis so that the results can be compared to experimental data. *Figure 1(b)* shows the relative position of the ice and tube during the melting process. Since unlike most PCMs, the ice density is less than that of the liquid phase, the ice shell will move up as the ice melts. With other PCM materials, the solid PCM shell will move down during melting. In either cases, the movement causes part of the tube to be in contact with the solid PCM and the rest part of the tube to be separated from the solid–liquid interface by a melted pool. To facilitate discussion of the problem, “contact region” will indicate the part of tube contacting the solid PCM, and “remote region” will indicate the part of the tube separated from

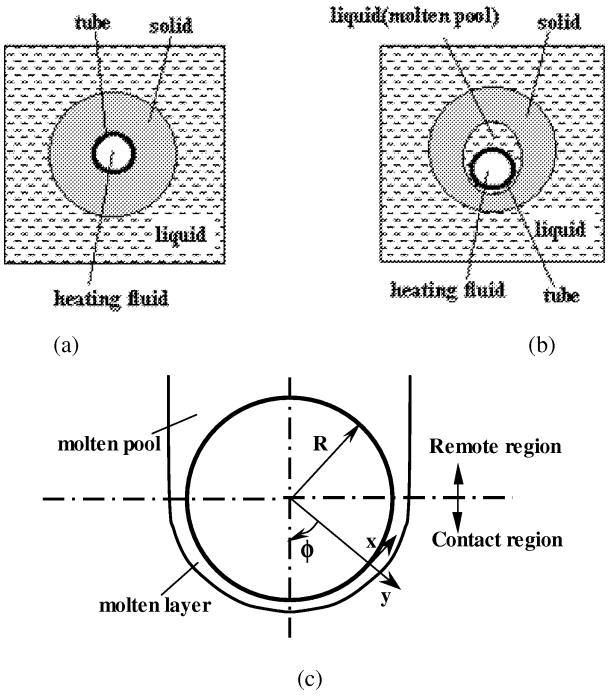

Figure 1. Physical model and coordinates.

the solid PCM by a melted pool, *figure 1*. *Figure 1(c)* illustrates the coordinates used for analyzing the ice-melting process. *Figure 2* shows a photo of the cross-section of an ice shell after melting through.

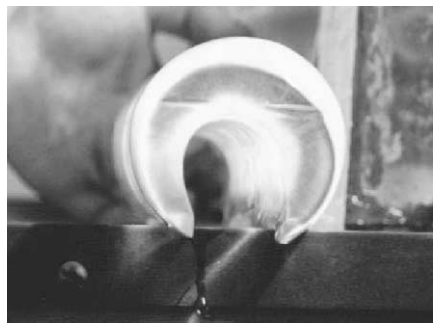

Figure 2. Photo of cross-section of an ice shell after melting through.

3. HEAT TRANSFER ANALYSIS BEFORE SOLID PCM IS PENETRATED

3.1. Melting process of the contact region before the solid PCM is penetrated

3.1.1. Energy balance of the melted layer

The analysis of the solid PCM melting process is divided into many short time periods (e.g., 10 or 30 s). Each time period $\Delta\tau$ (from τ^n to τ^{n+1}) uses a quasi-steady analysis, which assumes that $U^n = \mathrm{d}S^n/\mathrm{d}\tau$, the solid PCM velocity (upward for ice and downward for common PCMs), is constant over the short period, and the melted layer separating the tube and the solid PCM is very thin (i.e. $\delta/R \ll 1$). With these assumptions, the lubrication approximation [23] can be used to analyze contact region, since if $\delta/R \ll 1$ and $(\delta/R)Re_\mathrm{m} \ll 1$ (Re_m is the Reynolds number in the melt layer), the inertial terms can be neglected and $\partial^2/\partial x^2 \ll \partial^2/\partial y^2$.

Hence, the Navier–Stokes equation simplifies to

$$\mu\frac{\partial^2 u}{\partial y^2} = \frac{\mathrm{d}p}{\mathrm{d}x} \tag{1}$$

and the energy equation simplifies to

$$u\frac{\partial T}{\partial x} + v\frac{\partial T}{\partial y} = a\frac{\partial^2 T}{\partial y^2} \tag{2}$$

The boundary conditions at the tube surface are

$$u = v = 0, \quad T = T_\mathrm{w} \quad \text{when } y = 0 \tag{3}$$

The analysis also assumes that throughout the whole melting process, the solid PCM shell is at the melting point, T_m. The solid–liquid interface position is assumed to be fixed during time interval $\Delta\tau$, so that the melted solid mass is equal to the liquid mass melting from the solid–liquid interface with the boundary condition at the solid–liquid interface

$$u = 0, \quad v = -U^n\rho^*\cos\phi, \quad T = T_\mathrm{m} \quad \text{when } y = \delta \tag{4}$$

and

$$\left.\frac{\partial T}{\partial y}\right|_{y=\delta} = -\frac{\rho_\mathrm{s}U^n}{k_\mathrm{l}}h_\mathrm{fus}\cos\phi \tag{5}$$

Combining equation (1) with the boundary conditions (3) and (4) yields:

$$u = \frac{1}{2\mu}\frac{\mathrm{d}p}{\mathrm{d}x}y(y-\delta) \tag{6}$$

Using mass conservation to relate the pressure gradient and the melted layer thickness and designating the average velocity of the melted layer as $\overline{u}$ where the angle ϕ is defined in *figure 1* gives:

$$\rho^* U^n RL \sin\phi = L\delta\overline{u} \tag{7}$$

Equation (6) and the definition of the average velocity $\overline{u}$ give

$$\overline{u} = \frac{1}{\delta}\int_0^\delta u \, \mathrm{d}y = -\frac{1}{12\mu}\frac{\mathrm{d}p}{\mathrm{d}x}\delta^2 \tag{8}$$

Combining equations (7) and (8) gives

$$\frac{\mathrm{d}p}{\mathrm{d}x} = -\frac{12\mu R\rho^* U^n}{\delta^3}\sin\phi \tag{9}$$

Combining equations (9) and (6) gives:

$$u = -6\rho^* U^n Ry(y-\delta)\frac{\sin\phi}{\delta^3} \tag{10}$$

Combining equation (2) with the continuity equation and integrating, using the boundary conditions (3) and (4), gives:

$$\frac{\mathrm{d}}{\mathrm{d}x}\int_0^\delta uT \, \mathrm{d}y - \rho^* U^n T_\mathrm{m}\cos\phi = a\left(\left.\frac{\partial T}{\partial y}\right|_{y=\delta} - \left.\frac{\partial T}{\partial y}\right|_{y=0}\right) \tag{11}$$

The temperature distribution in the liquid gap separating the tube and the solid PCM in the y direction is approximated by

$$T = A + By + Cy^2 \tag{12}$$

With the boundary conditions (3)–(5), the temperature distribution is

$$T = T_\mathrm{w} + y\left[-\frac{2(T_\mathrm{w}-T_\mathrm{m})}{\delta} + \frac{\rho_\mathrm{s} U^n h_\mathrm{fus}}{k_\mathrm{l}}\cos\phi\right] + y^2\left[\frac{(T_\mathrm{w}-T_\mathrm{m})}{\delta^2} - \frac{\rho_\mathrm{s} U^n h_\mathrm{fus}}{k_\mathrm{l}\delta}\cos\phi\right] \tag{13}$$

Inserting equations (5), (10) and (13) into equation (11) gives

$$\frac{\mathrm{d}}{\mathrm{d}\phi}\left(\Delta^*\sin 2\phi\right) + \frac{20+3Ste}{U^{n*}}\cos\phi - \frac{20Ste}{U^{n*2}\Delta^*} = 0 \tag{14}$$

where $\Delta^* = \delta/R$, $Ste = c_p(T_\mathrm{w}-T_\mathrm{m})/h_\mathrm{fus}$, and $U^{n*} = \rho^* U^n R/a$ with the boundary condition $\mathrm{d}\Delta^*/\mathrm{d}\phi = 0$ at $\phi = 0$.

Equation (14) relates Δ^* and ϕ. However, equation (14) is very difficult to be solved analytically. Assuming a relationship between Δ^* and ϕ of the form

$$\Delta^*\cos\phi = \text{const} \tag{15}$$

inserting equation (15) into equation (14), the solution is

$$\Delta^* = \frac{f(Ste)}{U^{n*}\cos\phi} \tag{16}$$

where

$$f(Ste) = \frac{1}{4}\left[\left(400 + 280Ste + 9Ste^2\right)^{1/2} - 20 - 3Ste\right] \tag{17}$$

Expression (16) is applicable only for angles from 0 to ϕ_cri, where ϕ_cri satisfies the condition $\delta(\phi_\mathrm{cri})/R = \Delta^*(\phi_\mathrm{cri}) \ll 1$ which is the basis for the derivation. It is further assumed that the melted layer thickness becomes constant, i.e. $\Delta^* = \Delta^*(\phi_\mathrm{cri})$ for angles $\phi_\mathrm{cri} \le \phi \le \pi/2$ is consistent with the assumption $\delta/R \ll 1$. *Figure 3* shows the relationship between the tube and the solid–liquid interface. Curve A–B–C illustrates equation (16), while curve A–B–D represents the solid–liquid interface in this model. Usually, ϕ_cri can be determined by $\Delta^*(\phi_\mathrm{cri}) = 0.1$.

The solid PCM velocity is determined by balancing the forces on the solid PCM. The gravitational force acting on the solid PCM should be balanced by the pressure of the liquid in the gap. Experimental results showed that the melted solid PCM volume in the remote

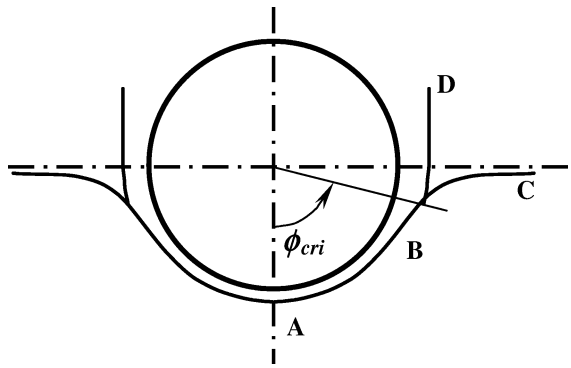

Figure 3. Shape of the ice melt interface with amplified melted layer.

region is relatively small. Neglecting the effect of molten volume in the remote region, the force balance is

$$\Delta\rho\pi g\left(R_s^2 - R^2 - S^n\frac{2R}{\pi}\right)L = 2L\int_0^{\phi_{cri}}(p\cos\phi + \tau_{yx}\sin\phi)R\,d\phi \quad (18)$$

where $\Delta\rho = |\rho_l - \rho_s|$ and S^n is the movement at time $\tau = \tau^n$, $S^n = S^{n-1} + U^{n-1}\Delta\tau$, $n = 1, 2, \ldots$ and $S^0 = 0$, and τ_{yx} is the shear stress which can be neglected compared to the pressure if $\delta/R \ll 1$. Therefore, equation (18) becomes

$$\Delta\rho\pi g\left(R_s^2 - R^2 - S^n\frac{2R}{\pi}\right)L = 2LR\int_0^{\phi_{cri}} p\cos\phi\,d\phi \quad (19)$$

Further assuming that $p = 0$ at $\phi = \phi_{edge}$ and inserting equation (16) into equation (9) gives

$$p = \frac{3\mu R^2 U^{n4}\rho^{*4}}{a^3 f^3(Ste)}\cos^4\phi \quad (20)$$

Inserting equation (20) into equation (19) gives the dimensionless solid PCM velocity during the period from τ^n to τ^{n+1}

$$U^{n*} = \frac{\rho^* U^n R}{a} = \left[\frac{5\pi\Delta\rho g R(R_s^2 - R^2 - 2S^n R/\pi)f^3(Ste)}{16\alpha\rho_l\nu}\right]^{0.25} \quad (21)$$

Combining equations (13) and (16) gives the heat flux at the tube surface:

$$q'' = -k_l\left.\frac{\partial T}{\partial y}\right|_{y=0} = \rho_s U^n h_{fus}\left(\frac{2Ste}{f(Ste)} - 1\right)\cos\phi \quad (22)$$

The total heat transfer in the contact region of the tube during time interval $\Delta\tau$ is found by integrating equation (22) over $0 \le \phi \le \phi_{cri}$:

$$q_{contact}^n = 2LR\rho_s U^n h_{fus}\left[\frac{2Ste}{f(Ste)} - 1\right]\sin\phi_{cri} + \Delta q \quad (23)$$

where

$$\Delta q = \frac{k_l L(T_w - T_m)(\pi/2 - \phi_{cri})}{\ln(1 + \Delta^*(\phi_{cri}))}$$

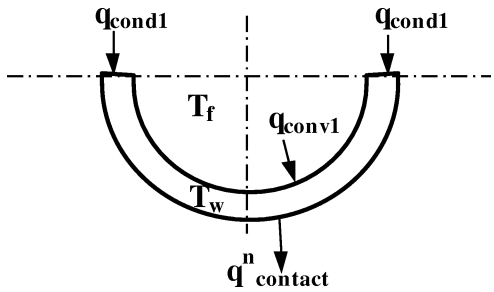

Figure 4. Energy balance for the tube contact region.

3.1.2. Tube energy balance

The tube wall temperature T_w plays an important role in the Stephan number *Ste* for the heat transfer below the tube. T_w can be determined from energy balance on the tube.

Before the solid PCM is penetrated, a liquid film is maintained between the tube and the solid PCM, while the remote region of the tube is isolated from the solid PCM by a growing liquid pool. Therefore, the wall temperature of the remote region of the tube can be assumed to be higher than the temperature in the contact region, so heat is conducted along the tube wall from the remote region to the contact region along the perimeter. The liquid film between the tube and the solid PCM is so thin that the temperature of the contact region of tube wall can be regarded as uniform. *Figure 4* shows the energy balance for the contact region of the tube.

From *figure 4*, the energy balance for the tube wall is

$$h_i\pi R_i\left[T_f - T_w\left(\phi < \frac{\pi}{2}\right)\right] + \frac{2L\delta_w k_w}{LR}\left.\frac{dT_w}{d\theta}\right|_{\theta=0} = 2R\rho_s U^n h_{fus}\left[\frac{2Ste}{f(Ste)} - 1\right] \quad (24)$$

3.2. Heat conduction through the melted pool in the remote region

The heat transferred through the melted pool, although much less than that in the contact region, may account for a significant portion of the total heat transfer in the beginning because the solid–liquid interface is very near to the tube surface.

For most PCMs, the molten pool is below the tube, the heating surface is above the molten PCM and the liquid density decreases with temperature increasing. Therefore, it is justified for this model assuming that the heat transfer in the remote region is pure conduction.

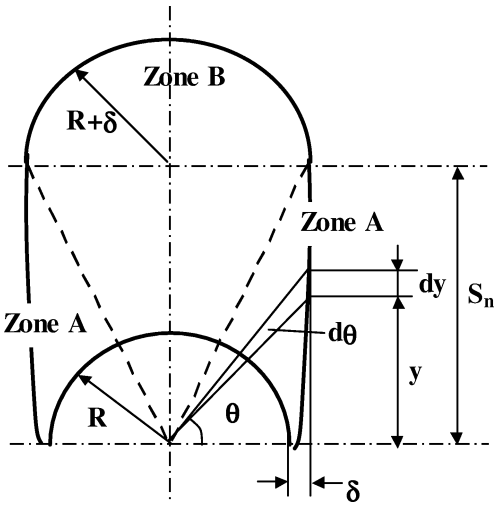

Figure 5. Geometry of the melted pool in the remote region during ice melting.

Correction may be necessary for ice–water due to the maximum density of water at 4 °C. Further discussion will deal with this problem in the section of model validation.

Figure 5 illustrates the geometry of the melted pool in the remote region during the ice melting process. The melted pool can be divided into two parts by the dotted lines for $\theta = \arctan[S^n/(R+\delta)]$: the side zone A and top zone B.

3.2.1. Heat conduction in zone A

Zone A is in the region $0 \le \theta \le \arctan[S^n/(R+\delta)]$. The wall temperature varies along the tube perimeter as the distance between the tube and the solid PCM shell varies, while the wall temperature difference in the radial direction can be ignored because the local Biot number is smaller than 0.1. Therefore, the conductive heat transfer rate in an element of $\mathrm{d}\theta$ (or $\mathrm{d}y$) is

$$q_1 = \frac{k_\mathrm{l} L(T_\mathrm{w} - T_\mathrm{m})\,\mathrm{d}\theta}{\ln[(1+\delta/R)/\cos\theta]} \tag{25}$$

From *figure 6*, the energy balance in a tube wall element can be expressed as

$$\frac{\delta_\mathrm{w} k_\mathrm{w}}{R}\frac{\mathrm{d}^2 T_\mathrm{w}}{\mathrm{d}\theta^2} - \left[\frac{k_\mathrm{l}}{\ln[(1+\delta/R)/\cos\theta]} + h_\mathrm{i} R_\mathrm{i}\right] T_\mathrm{w} + \frac{k_\mathrm{l} T_\mathrm{m}}{\ln[(1+\delta/R)/\cos\theta]} + h_\mathrm{i} R_\mathrm{i} T_\mathrm{f} = 0 \tag{26}$$

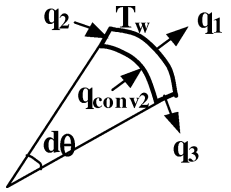

Figure 6. Energy balance of tube wall of zone A.

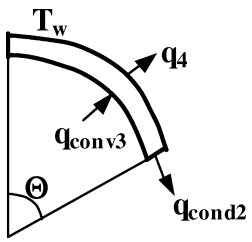

Figure 7. Energy balance of tube wall of zone B.

The energy balance for the melted solid gives

$$q_1 = \rho_\mathrm{s}\,\mathrm{d}y\,Lh_\mathrm{fus}\frac{\mathrm{d}\delta}{\mathrm{d}\tau} \tag{27}$$

The geometry in *figure 5* shows that $\mathrm{d}\theta$ can be expressed as

$$\mathrm{d}\theta = \frac{(R+\delta)\,\mathrm{d}y}{(R+\delta)^2 + y^2} \tag{28}$$

Combining equations (25), (27) and (28), the melting rate of the solid in zone A can be written as

$$\frac{\mathrm{d}\delta}{\mathrm{d}\tau} = \frac{k_\mathrm{l}(T_\mathrm{w} - T_\mathrm{m})(R+\delta)}{\rho_\mathrm{s} h_\mathrm{fus}\ln[(1+\delta/R)/\cos\theta][(R+\delta)^2 + y^2]} \tag{29}$$

3.2.2. Heat conduction in zone B

Zone B is in the region $\theta > \arctan[S^n/(R+\delta)]$. The distance between the tube and solid–liquid interface is almost uniform, so a lumped temperature assumption is used for this part of the tube wall. The heat transfer between the tube and the solid–liquid interface in zone B can be approximated by heat conduction between concentric cylinders (*figure 7*):

$$q_4 = \frac{\Theta k_\mathrm{l} L(T_\mathrm{f} - T_\mathrm{m})}{\ln[1 + (\delta + S^n)/R]} \tag{30}$$

where

$$\Theta = \frac{\pi}{2} - \arctan\frac{S^n}{R+\delta}$$

is the angular extent of zone B.

An energy balance for the tube wall in zone B yields:

$$h_i R_i (T_f - T_w) = \frac{k_l T_w}{\ln[1 + (\delta + S^n)/R]} + \frac{L\delta_w k_w}{L\Theta R} \frac{dT_w}{d\theta}\bigg|_{\theta=\arctan[S^n/(R+\delta)]}$$

The tube wall temperature is then

$$T_w = \frac{h_i R_i T_f - \frac{L\delta_w k_w}{L\Theta R} \frac{dT_w}{d\theta}\big|_{\theta=\arctan[S^n/(R+\delta)]}}{k_l/\ln[1 + (\delta + S^n)/R] + h_i R_{int}} \quad (31)$$

The melting rate for the solid–liquid interface in zone B is

$$\frac{d\delta}{d\tau} = \frac{\Theta k_l (T_w - T_m)}{\ln[1 + (\delta + S^n)/R]\rho_s h_{fus} \pi (R + \delta)/2} \quad (32)$$

4. ANALYSIS OF THE HEAT TRANSFER AFTER THE SOLID IS PENETRATED

4.1. Heat transfer in the contact region

Since the contact surface area decreases after the solid PCM shell is penetrated, the latent heat transfer area decreases. The integration domain for equation (19) should be changed to $\phi_0 < \phi < \pi/2$:

$$\Delta\rho\pi g\left(R_s^2 - R^2 - S^n \frac{2R}{\pi}\right)L = 2LR\int_{\phi_0}^{\phi_{cri}} p\cos\phi \, d\phi \quad (33)$$

where ϕ_0 is defined as

$$\phi_0 = \arccos\left(\frac{R - \delta_l}{R}\right) \quad (34)$$

and $\delta_l = (R_s^2 - R^2 - S^{n2})/(2S^n)$, *figure 8*. When $S^n = \sqrt{R_s^2 - R^2}$, the penetrated solid PCM shell leaves the tube, and the process is considered to be terminated.

Substituting equation (20) into equation (33) yields

$$U^{n*} = \frac{\rho^* U^n R}{a} = \left[\frac{5\pi\Delta\rho g R(R_s^2 - R^2 - 2S^n R/\pi) f^3(Ste)}{16 h \rho_l \nu}\right]^{0.25} \cdot \xi(\phi_0) \quad (35)$$

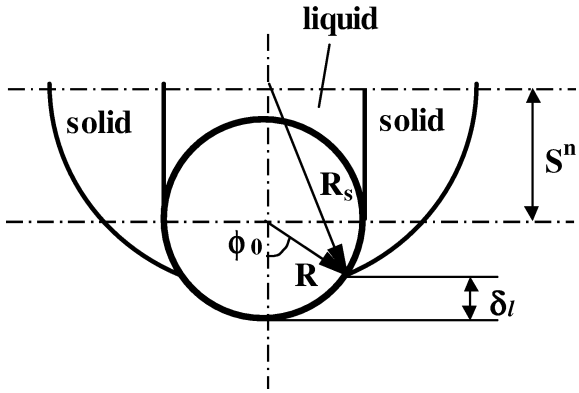

Figure 8. Schematic of relative location of the ice and tube when the ice is penetrated.

where

$$\xi(\phi_0) = \left[\frac{3}{8}\left(\sin^4\phi_0 + 4 - \frac{4}{3}\cos^2\phi_0\right)\cos\phi_0\right]^{-1/4}$$

Note that $\xi(\phi_0) \geq 1$ which indicates that after the PCM solid shell is penetrated the solid PCM velocity is faster than that before the penetration.

Integrating equation (22) over $\phi_0 < \phi < \phi_{cri}$, the total heat transfer from the heating fluid to the solid in the contact region along the tube from τ^n to τ^{n+1} is

$$q^n_{contact} = 2LR\rho_s U^n h_{fus}\left[\frac{2Ste}{f(Ste)} - 1\right]\sin\phi_{cri}(1 - \sin\phi_0) + \Delta q \quad (36)$$

where

$$\Delta q = \frac{k_l L(T_w - T_m)(\pi/2 - \phi_{cri})}{\ln[1 + \Delta^*(\phi_{cri})]}$$

4.2. Tube wall temperature determination

In this period, the heat transfer process is much more complicated. In the contact region, heat from the tube is partly transferred to the solid and partly to the free liquid outside of the tube and solid which differs from the heat transfer before the PCM was penetrated. After the solid is penetrated, the solid PCM moves up/down faster than before. As the solid PCM moves, the free liquid flows into the melted pool area, which enhances the heat convection in the melted pool in the remote region. Therefore, in this period, the tube wall temperature cannot be determined theoretically as in the former period.

TABLE I
Convection heat transfer coefficients used for the model.

Flow type	Heat transfer coefficient	Condition	Refs.
Laminar in a tube	$Nu_f = 1.86(Pe_f d/L)^{1/3}(\mu_f/\mu_w)^{0.14}$	$Re_f < 2\,300$, $0.48 < Pr_f < 16\,700$ and $0.0044 < (\mu_f/\mu_w) < 9.75$	[24]
Laminar in a tube	$Nu_f = 4.36$ (constant heat flux) $Nu_f = 3.66$ (constant surface temperature)	$[(Re_f Pr_f d/L)^{1/3}(\mu_f/\mu_w)] \leq 2$	[24]
Transition in a tube	$Nu_f = 0.012(Re_f^{0.87} - 280)Pr_f^{0.4}[1 + (d/L)^{2/3}](Pr_f/Pr_w)^{0.11}$	$2\,300 < Re_f < 10^4$, $5 < Pr_f < 500$ and $0.05 < Pr_f/Pr_w < 20$	[24]
Turbulent in a tube	$Nu_f = 0.023Re_f^{0.8}Pr_f^{0.3}$	$Re_f > 10^4$, $L/d \geq 10$ and $Pr_f = 0.7$–160	[24]
Natural convection around a horizontal tube	$Nu_l = 0.53(Gr\,Pr)^{0.25}$		[25]

As soon as the penetrated solid PCM leaves the tube, the tube wall temperature variation can be determined by assuming that the tube is immersed in liquid whose temperature is T_m. Natural convection heat transfer around a horizontal column is calculated using formulas from literature.

The change rate of T_w will increase with time because more free liquid flows into the melted layer which will increase the rate of change. Therefore, the tube wall temperature variation during the period from penetration of the solid to the departure of the solid from the tube was modeled using a quadratic function for the tube wall temperature variation:

$$T_w = T_{w1} + \frac{T_{w2} - T_{w1}}{\Delta\tau_{last}^2}\Delta\tau^2 \qquad (37)$$

where T_{w1} is the tube wall temperature of the contact region when the solid is penetrated, T_{w2} is the tube wall temperature when the tube is immersed in liquid at temperature T_m, $\Delta\tau_{last}$ is the time interval for which this period lasts, and $\Delta\tau$ is the time interval after the solid is penetrated.

4.3. Melting rate $d\delta/d\tau$ of solid PCM in the remote region after the solid is penetrated

In this period, the volume of the melted pool in the remote region expands faster than before due to the higher U_0^n value, which decreases the melting rate in this period. However, liquid flowing in from the external space will enhance convection in the melted pool which may compensate for the decreased melting rate. Therefore, the melting rate $d\delta/d\tau$ can be assumed to be constant after the solid is penetrated.

5. CONVECTIVE HEAT TRANSFER COEFFICIENTS

See *table I*.

6. EXPERIMENT

The experiments used a glass box containing a nickel coated cast iron tube of length 295 mm, *figure 9*. The

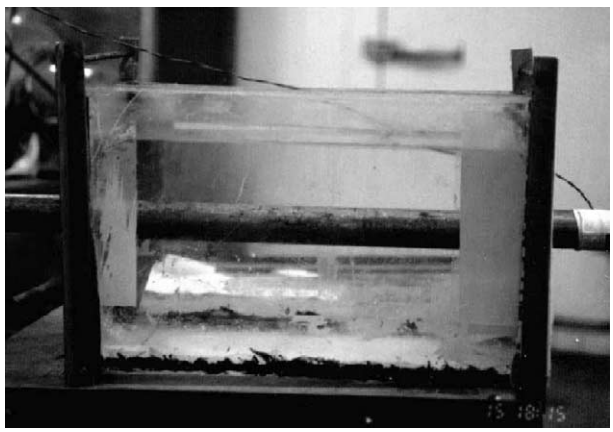

Figure 9. Experimental water tank.

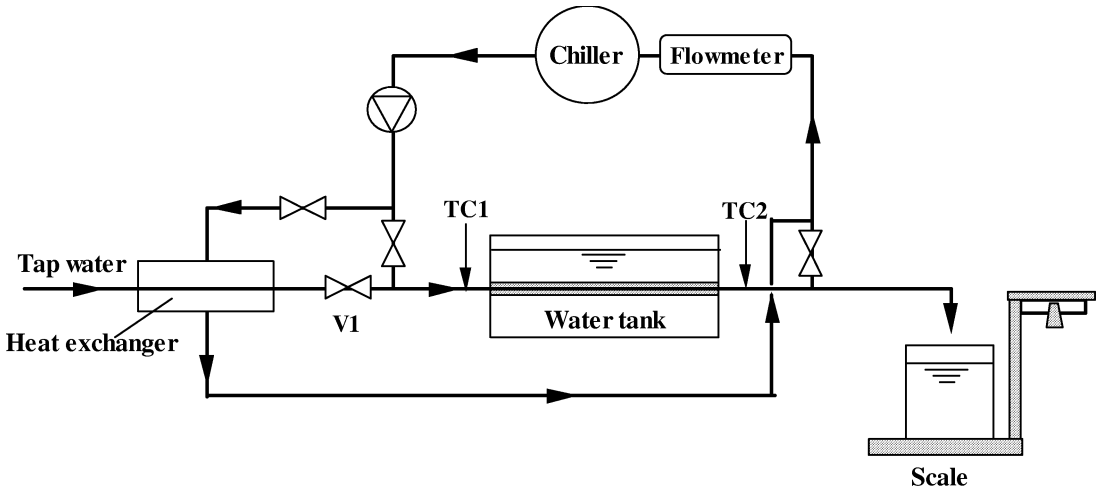

Figure 10. Experimental system schematic.

outside tube diameter was 26 mm and the inner diameter 20 mm. The glass box was $140 \times 140 \times 295$ mm^3. The water level in the glass box was 130 mm at 15 °C and the distance between the tube axis and the tank bottom was 65 mm.

Copper–constantan thermocouples with 0.1 K measurement accuracy were fixed on the external surfaces of the tube inlet and outlet and covered with insulation (TC1 and TC2 in *figure 10*). The water flow rate was measured by the weighting method. The scale accuracy was 0.05 kg. The water valve opening (V1 in *figure 10*) was fixed during the melting process. The time interval was recorded by a stopwatch with accuracy of 0.2 s. The inlet and outlet water temperatures were recorded by a HP34970 data logger every 10 s. The size of the ice was measured using a vernier calliper whose measurement accuracy was 0.1 mm.

During the ice formation process, the cooling fluid was a glycol solution of 30 %wt concentration whose inlet temperature was −7 °C and a flow rate of 0.4 m^3·h^{-1}. The flowmeter accuracy for measuring the secondary fluid flow rate was 0.5 %. The ice was melted by switching the cooling fluid to water whose inlet temperature was controlled at different levels. The experimental system is shown schematically in *figure 10*.

The melting experiments were conducted at different inlet temperatures and flow rates. The measured parameters for the four melting cases are listed in *table II*. The temperature measured by the thermocouples fixed to the tube surfaces of the inlet and outlet were used as the inlet and outlet secondary fluid temperatures. The average water temperature in *table II* was calculated from the measured inlet and outlet temperatures.

TABLE II
Experimental conditions.

Case	Inlet water temperature (°C)	Average water temperature (°C)	Average flow rate (kg·h^{-1})
1	9.5	9.3	160
2	9.5	8.6	50
3	15.0	14.7	240
4	15.0	14.7	160

TABLE III
Time interval from when melting process started.

Case	To when ice was penetrated (min)	To when ice left the tube (min)
1	–	11.0
2	13.0	16.0
3	4.5	6.0
4	6.5	8.5

The times for melting starting and ending were recorded by the stopwatch. The time when the water valve (i.e. V1 in *figure 10*) was opened was recorded as the melting starting time. The time when the ice shell left the tube and ascended to the water surface was recorded as the ending time. The time for the ice cylinder to penetrate was also recorded but the value was not very exact because the penetrating started from one end of the ice cylinder and was not easy to be detected immediately. *Table III* lists the time intervals from when

TABLE IV
Ice size before and after melting.

Case	Thickness before melting (mm)				Thickness after melting (mm)			Thickness of melted area (mm)		
	Lower	Upper	Left	Right	Upper	Left	Right	Upper	Left	Right
1	15.4	30.8	24.9	25.1	28.6	22.4	22.8	2.2	2.5	2.3
2	15.0	30.4	24.4	24.7	26.9	20.2	20.8	3.5	4.2	3.9
3	15.6	31.0	25.3	25.6	29.4	23.5	23.9	1.6	1.8	1.7
4	15.8	31.2	25.6	25.8	29.4	23.6	24.0	1.8	2.0	1.8

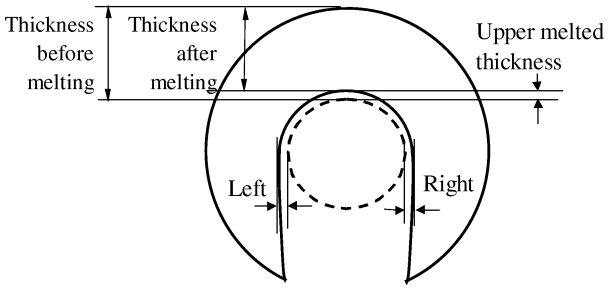

Figure 11. Measured positions of the ice shell as it departured from the tube. The dotted line shows the original relative position of the tube.

TABLE V
Melted ice volume ($m^3 \cdot 10^6$).

Case	1	2	3	4
Total melted volume	141	153	136	139
Melted volume of contact region	118	115	120	121
Ratio of the melted volume of remote region over the total melted volume (%)	15.9	24.7	12.0	12.8
Ratio of the melted volume of contact region over the total melted volume (%)	84.1	75.3	88.0	87.2

melting started to the moment when the ice cylinder was penetrated and to the moment when the ice shell left the tube.

The ice size was measured before and after the melting process, *table IV*. The thickness of the melted area listed in *table IV* was measured at the positions shown in *figure 11*. The volumes of the melted ice region were calculated for the four test cases, *table V*. The actual discharge capacity can be obtained from the melted ice volume

$$Q = \rho_s V h_{fus} \tag{38}$$

7. PHOTOGRAPHIC EXPERIMENTAL RESULTS

The melting processes for cases 2, 3 and 4 were recorded photographically. *Figure 12* shows the photos of the melting process for case 4. Time interval for the whole melting process: 18:00:50–18:09:20. Time when the ice cylinder started to be penetrated: 18:07:20. The times in the brackets of the subtitles of *figure 3* were the times recorded in the photos by the camera timer. The error of the camera timer display is ± 30 s. The numbers displayed in the photo were date-hour-minute.

8. COMPARISON BETWEEN SIMULATION AND EXPERIMENTS

Tables VI and *VIII* list the simulated and experimental results. Only the time elapsed for the melting process and the melted ice size are compared. The temperature measurement accuracy was 0.1 K and the temperature difference between the inlet and the outlet of the secondary fluid was about 0.5 K, so the relative error of the heat flux calculated using this measured temperature difference was so large that it is not listed here. In contrast, the time for the melting process was recorded with much less relative error and accurately reflects the heat flux.

The data in *table VI* show that the simulation results for the duration of the melting process agrees well with the experiments. The relative errors of the model from the experiments are less than 15 %. The data in *table VI* also show that all of the predicted processes are faster than the experimental processes. The reasons may be:

(1) The initial ice temperature was not at T_m, 0 °C, but lower than 0 °C because the melting experiments were started just after the ice formation.

(2) Experimental error.

Table VII shows the estimated sensible heat effect on the melting process. The average outer radius of the

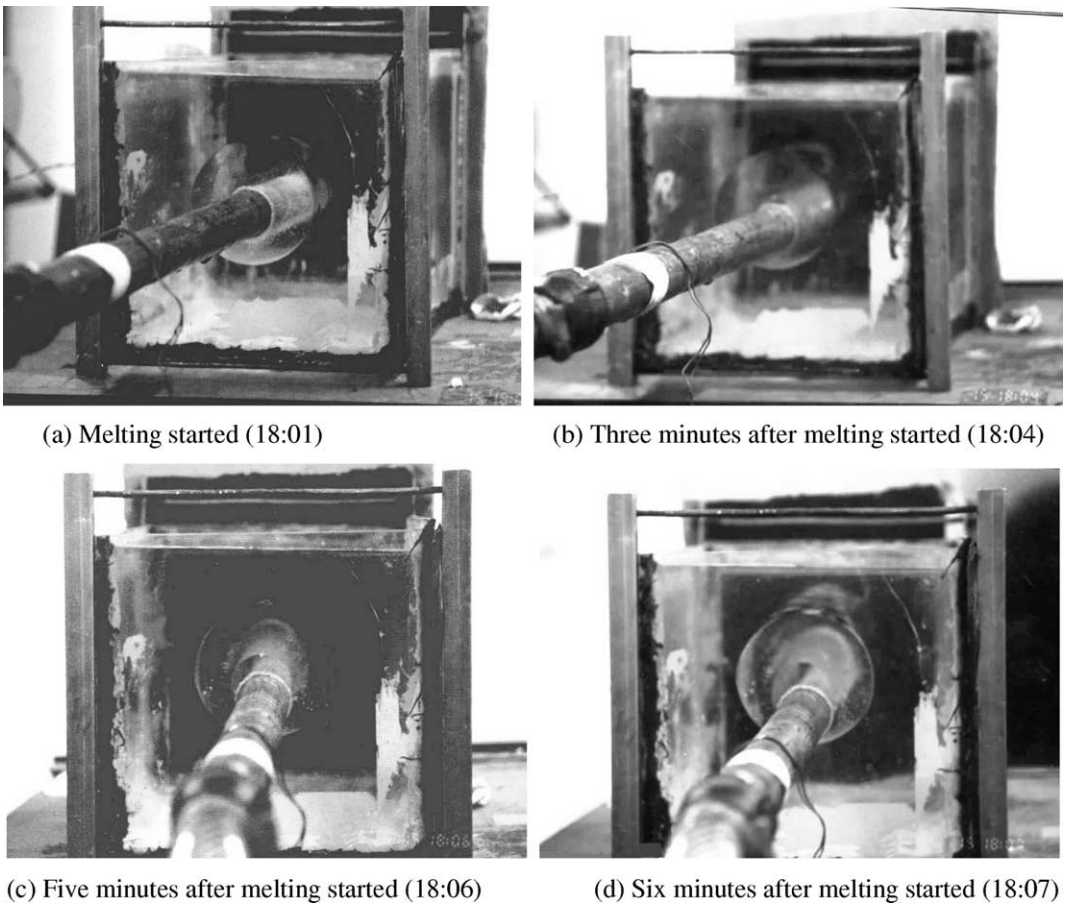

Figure 12. Photos of the ice melting process for case 4.

TABLE VI
Comparison of the calculated and measured duration of the melting processes.

Case	Time interval from beginning to ice penetration			Time interval from beginning to ice departure from the tube		
	Experiment (min)	Simulation (min)	Relative error (%)	Experiment (min)	Simulation (min)	Relative error (%)
1	–	8.14	–	11.0	10.8	1.82
2	13.0	11.1	14.8	16.0	14.2	11.4
3	4.5	3.9	13.3	6	5.47	8.83
4	6.5	5.82	10.5	8.5	7.84	7.76

TABLE VII
Improved estimate of the time intervals from the beginning to the moment when the ice departured from the tube considering the ice sensible heat.

Case	Experiment (min)	Simulated latent heat transfer (min)	Sensible heat transfer estimate (min)	Total estimated time interval (min)	Deviation (%)
1	11	10.8	0.83	11.63	−5.7
2	16	14.21	1.16	15.37	3.9
3	6	5.47	0.39	5.86	2.3
4	8.5	7.84	0.57	8.41	1.0

(e) Seven minutes after melting started (18:08)

(f) Eight minutes after melting started (18:09)

(g) 8.5 minutes after melting starting (18:09)

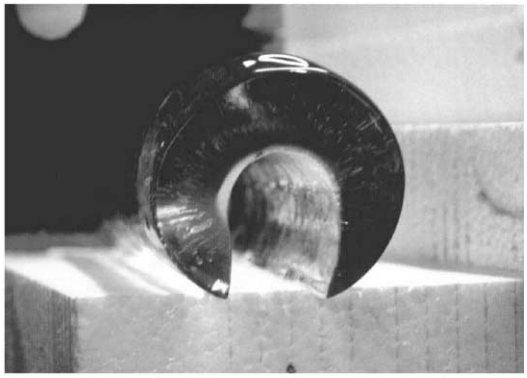

(h) Ice shell that left the tube (18:10)

Figure 12. (continued).

TABLE VIII
Melt thickness at the side and top of the ice internal surface.

Case	Melt thickness at the side			Melt thickness at the top		
	Experiment (mm)	Simulation (mm)	Deviation (%)	Experiment (mm)	Simulation (mm)	Deviation (%)
1	2.4	1.98	18	2.2	1.76	20.0
2	4.1	1.94	52	3.5	1.74	50.3
3	1.8	2.04	−17	1.6	1.8	−12.5
4	1.9	2.01	−5.8	1.8	1.78	1.1
Average	2.5	1.99	21.1	2.28	1.77	22.2
Average of cases 1, 3 and 4	2.02	2.01	0.3	1.87	1.78	4.6

ice cylinders for the four test cases was about 36.3 mm and the outer tube radius was 13.0 mm. Therefore, the average initial ice volume was about 1 060 cm^3. The inlet temperature of the glycol solution was controlled at −7 °C. The temperature of the external ice cylinder surface would be 0 °C, so the sensible heat of the ice before melting was estimated to be about −3.48 kJ using a cylindrical conduction model. The average heat flux through the tube was used to estimate the time needed to remove this sensible heat from the ice during melting. It is found that if the sensible heat of the ice is considered, the deviations of the simulated time intervals from the experimental results for the entire melting process are reduced, *table VII*.

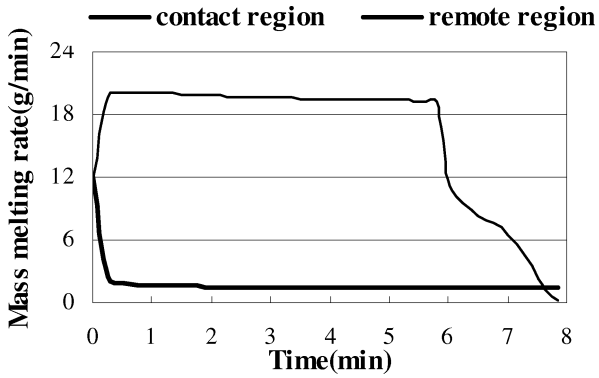

Figure 13. Predicted mass melting rate of case 4.

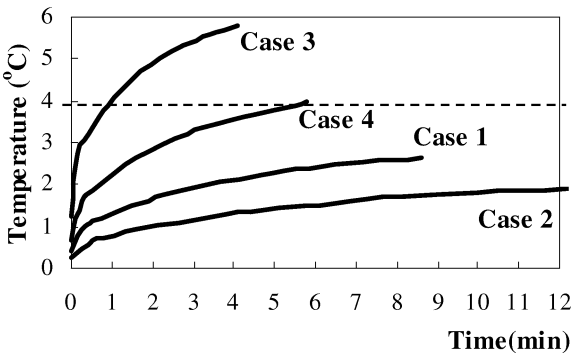

Figure 14. Predicted temperature at top of the tube during melting.

Table VIII lists the simulated melted ice thickness at the sides and top of the ice above the tube. The simulation results for case 1, 3 and 4 agree well with the experimental results, with relative errors are less than 20 %. However, the simulation results for case 2 are far away from the experimental results. It was perhaps due to the measurement error.

Figure 13 shows the comparison between the predicted mass melting rates in the remote region and the contact region for case 4. Combining *table V* and *figure 13*, only considering the melting rate in the contact region may result in 15 % error in melting rate prediction.

Figure 14 shows the simulation results for the temperature at top of the tube. It is found that the tube temperatures during melting were lower or not much higher than 4 °C. It is the reason why from the comparison between simulation and experiments, convection caused by water density variation seemed not effective. Another reason is that the melting rate of the remote region takes up less than 15 % of the overall melting rate, hence omitting the convection effect on heat transfer will not cause evident error.

9. CONCLUSIONS

A theoretical model is developed for the thermal process for melting of unfixed solid PCM outside a horizontal tube. The model is validated experimentally showing that the model is accurate enough to be used to predict the melting rate and the time needed to melt the solid PCM. The model can be used to optimize the design and operation of latent heat energy storage systems with PCM outside parallel tubes.

In the melt of an unfixed solid phase change material outside a horizontal tube, the heat transfer in the remote region can be regarded as pure conduction with the total heat transfer in this region being much smaller than that through the gap between the solid PCM and the tube in the remote part.

Measuring the duration of the melting of a solid PCM can greatly improve the measurement precision of the heat transfer instead of measuring the temperature difference between the fluid inlet and outlet.

The analytical results agree fairly well with the experimental results, which shows that the model is accurate enough to predict the solid PCM melting rate and the time needed to melt the solid PCM. The model can be used to optimize the design and operation of latent heat energy storage systems with PCM outside parallel tube.

REFERENCES

[1] Hale N.W. Jr., Viskanta R., Solid-liquid phase change heat transfer and interface motion in materials cooled or heated from above and below, Int. J. Heat Mass Tran. 23 (1980) 283-292.

[2] Hale N.W. Jr., Viskanta R., Photographic observation of a solid heated from an isothermal vertical wall, Lett. Heat Mass Tran. 5 (1978) 329-337.

[3] White R.D., Bathelt A.G., Viskanta R., Study of heat transfer and melting from a cylinder embedded in a phase change material, ASME Paper No. 77-HT-42, 1977.

[4] Bathelt A.G., Viskanta R., Leidenfrost W., Latent heat of fusion energy storage, experiments on heat transfer from cylinders during melting, J. Heat Tran. 101 (1979) 453-458.

[5] Bathelt A.G., Viskanta R., Heat transfer at the solid-liquid interface during melting from a horizontal cylinder, Int. J. Heat Mass Tran. 23 (1980) 1493-1503.

[6] Viskanta R., Bathelt A.G., Hale N.W., Latent heat-of-fusion energy storage: Experiments on heat transfer during solid-phase change, in: Proc. 3rd Int. Conf. on Alternative Energy Sources, Bal Harbour, FL, 1980.

[7] Rieger H., Projahn U., Beer H., Analysis of the heat transport mechanisms during melting around a horizontal circular cylinder, Int. J. Heat Mass Tran. 25 (1982) 137-147.

[8] Bareiss M., Beer H., Influence of natural convection on the melting process in a vertical cylindrical enclosure, Lett. Heat Mass Tran. 7 (1980) 329–338.

[9] Pannu J., Joglekar G., Rice P.A., Natural convection to cylinders of phase change material used for thermal storage, in: AIChE Symp. Ser., 1980, pp. 47–55.

[10] Katayama K., Saito A. et al., Heat transfer characteristics of the latent heat thermal energy storage capsule, Solar Energy 27 (1981) 91–97.

[11] Rieger H., Projahn U. et al., Heat transfer during melting inside a horizontal tube, J. Heat Tran. 105 (1983) 226–234.

[12] Bahrami P.A., Wang T.G., Analysis of gravity and conduction-driven melting in a sphere, Trans. ASME 109 (1987) 806–809.

[13] Yaojiang H., Mingheng S., Analysis of contact melting of PCM in a spherical capsule, Chinese Science Ser. E 28 (1) (1998) 51–55.

[14] Moalemi M.K., Viskanta R., Analysis of close contact melting heat transfer, Int. J. Heat Mass Tran. 29 (1986) 855–867.

[15] Moalemi M.K., Viskanta R., Analysis of melting around a moving heat source, Int. J. Heat Mass Tran. 29 (1986) 1271–1282.

[16] Moalemi M.K., Webb B.W., Viskanta R., An experimental study of close contact melting, ASME J. Heat Tran. 108 (1986) 894–899.

[17] Webb B.W., Moalemi M.K., Viskanta R., Experiments on melting of unfixed ice in a horizontal cylindrical capsule, ASME J. Heat Tran. 109 (1987) 454–459.

[18] Nicholas D., Bayazitoglu Y., Thermal storage of phase change material in horizontal cylinder, in: Proceedings of the 3rd Miami International Conference on Alternative Energy Sources, Miami Beach, FL, USA, Vol. 1, Solar Energy, 1983.

[19] Bareiss M., Beer H., Analytical solution of the heat transfer process during melting of an unfixed solid phase change material inside a horizontal tube, Int. J. Heat Mass Tran. 27 (5) (May 1984) 739–746.

[20] Wenzheng C., Shangmo C., Zhen L., Analysis of contact melting of PCM in a tube of oval cross section and in a tube of rectangular section, Acta Energiae Solaris Sinica 16 (1) (1994) 68–71.

[21] Wenzheng C., Shangmo C., Zhen L., Analysis of contact melting of PCM in a tube of rectangular cross section, Acta Energiae Solaris Sinica 15 (3) (1993) 202–208.

[22] Yang F., Experimental study on some problems about thermal characteristics of internal melt ice-on-coil tank, Master Degree Thesis, Tsinghua University, China, June 1999.

[23] Schlichting H., Boundary Layer Theory, 7th ed., McGraw-Hill, New York, pp. 108–114.

[24] Incropera F.P., Dewitt D.P., Fundamentals of Heat and Mass Transfer, 4th ed., Wiley.

[25] McAdams W.H., Heat Transmission, 3rd ed., McGraw-Hill, New York, 1954.